Biomedicine & Pharmacotherapy 68 (2014) 873–879

Available online at
ScienceDirect
www.sciencedirect.com

Elsevier Masson France
EM|consulte
www.em-consulte.com/en

Original article

Involvement of the NF-κB/p50/Bcl-3 complex in response to antiangiogenic therapy in a mouse model of metastatic renal cell carcinoma

Marina de Souza Braga [a,d], Katiúcia Batista da Silva Paiva [b], Karen Foguer [a,d], Karen Cristina Barbosa Chaves [a,d], Larissa de Sá Lima [c], Cristoforo Scavone [c], Maria Helena Bellini [a,d,*]

[a] Nephrology Division, Federal University of Sao Paulo, Sao Paulo, Brazil
[b] Department of Oral Pathology,Dental School, University of Sao Paulo, Sao Paulo, Brazil
[c] Department of Pharmacology, Institute of Biomedical Sciences, University of Sao Paulo, Sao Paulo, Brazil
[d] Biotechnology Department, IPEN-CNEN, Sao Paulo, Brazil

ARTICLE INFO

Article history:
Received 3 June 2014
Accepted 7 July 2014

Keywords:
Renal cell carcinoma
NF-κB
Bcl-3
p50
Endostatin

ABSTRACT

Renal cell carcinoma (RCC) represents approximately 2–3% of human malignancies. Nuclear transcription factor κB (NF-κB) is composed of a family of transcription factors that have been associated with the development and progression of RCC. Endostatin (ES) is a fragment of collagen XVIII that possesses antiangiogenic activity. In this study, we evaluated the expression of NF-κB in metastatic tumor cells from animals treated with ES. Balb/c-bearing Renca-EGFP cells were treated with NIH/3T3-LendSN or NIH/3T3-LXSN cells as a control. At the end of the in vivo experiment, plasma Renca-EGFP-sorted cells and tissue lung samples were collected. A real-time PCR array for NF-κB target genes revealed that ES therapy led to down regulation of Bcl-3 ($P < 0.031$), NF-κB1 ($P < 0.001$) and c-Rel ($P < 0.004$) in the ES-treated group. Using an electrophoretic mobility shift assay (EMSA), we observed a reduction in NF-kB binding activity in ES-treated Renca-EGP cells. Furthermore, a supershift assay showed a clear shift of the NF-κB DNA band in samples incubated with a p50 antibody. By immunohistochemistry analysis, ES treatment resulted in a significant reduction in expression of p50. (ES vs. control $P < 0.05$). The immunoprecipitation experiments confirmed the presence of a p50/Bcl-3 complex in nuclear extracts from cells of metastatic lung tissues. Our findings indicate that p50 and Bcl-3 plays a regulatory role in gene transcription in RCC.

1. Introduction

Renal cell carcinoma (RCC) is the most common renal cancer and accounts for 90–95% of kidney neoplasms [1]. This malignancy is clinically and pathologically heterogeneous, and clear cell renal carcinoma (ccRCC) the most common type in adults. Most cases of primary RCC are treated with partial or radical nephrectomy. However, the incidence of metastatic disease following surgery is approximately 40% [2]. The high incidence of metastatic disease has been associated with a RCC angiogenic phenotype, which results from a mutation or hypermethylation of the von Hippel-Lindau (VHL) gene, with subsequent hypoxia-inducible factor (HIF) activation. Overexpression of the HIF protein results in increased expression of vascular endothelial growth factor (VEGF) and platelet derived growth factor (PDGF), which are key players involved in ccRCC development and progression [3,4].

One of the molecules involved in the development and progression of RCC is the nuclear transcription factor κB (NF-κB). NF-κB is a pleiotropic transcription factor belonging to the Rel/NF-κB family that participates in the activation of many genes, including cytokines and metalloproteinases (MMPs) [5]. In mammals there are five known members of the Rel family: RelA (p65), RelB, c-Rel, NF-κB1 105/p50, and NF-κB2-p100/p52. NF-κB1-p105/p50 and NF-κB2-p100/p52 are precursor molecules that undergo cleavage of the N-terminal region in the proteasome, generating the mature proteins p50 and p52. These subunits homo or heterodimerize to form activator dimers (p50/p65) and repressors (p50/p50 and p52/p52) [6,7]. NF-κB dimers bind at a consensus sequence (IkB sites, 5′GGRRNNYYCC3′, R = purine Y = pyrimidine). Without stimulation, NF-κB remains in the

* Corresponding author at: Biotechnology Department, Nuclear and Energy Research Institute, Sao Paulo, Brazil Tel.: +551131339706.
E-mail addresses: mhmarumo@terra.com.br, mbmarumo@ipen.br (M.H. Bellini).

http://dx.doi.org/10.1016/j.biopha.2014.07.008
0753-3322/

cytoplasm in its inactive form linked to one of its inhibitors (IKBs), including IkB-α, IkB-β, IkB–ε, IkBγ, IkBδ and Bcl-3 [6].

The best-described NF-κB pathways are classical and alternative pathways or canonical and non-canonical pathways, respectively [7,8]. The canonical pathway is activated by inflammatory cytokines and viral infections. Upon activation of this pathway, IKB is phosphorylated, ubiquinated and hence degraded by the proteasome. Free NF-κB (p65 and p50) migrates to the nucleus where it activates transcription of specific genes. The non-canonical pathway is activated by members of the tumor necrosis factor (TNF) family, such as the B cell activating factor (BAFF) lymphotoxin B. In this pathway, IKKα is activated and subsequently phosphorylates p100. The p100 protein is ubiquinated and processed, yielding mature p52. Thus, the RelB/p52 heterodimer migrates to the nucleus where it activates transcription of specific genes [5,9]. According to Gilmore, other distinct pathways must exist. For example, the p50 homodimer together with Bcl-3 can act as a transcriptional activator [7]. Furthermore, an association between the NF-κB activator (the Bcl-3/p50 complex) and development of nasopharyngeal carcinoma has been shown [10].

Over the last decade, papers have correlated NF-κB activation with angiogenesis, chemotherapy resistance and apoptosis resistance in RCC. Oya et al. were the first to demonstrate constitutive activation of NF-κB in RCC cell lines using an electrophoresis mobility shift assay (EMSA). Moreover, high NF-κB activity was inversely correlated with TRAIL-induced apoptosis. Supershift assay results showed that p50 was involved [11]. The same group also studied NF-κB expression in RCC tissue samples and found a positive correlation between the histological grade, invasion, metastasis and inflammatory paraneoplastic syndrome by activating NF-κB [12].

Two independent groups, Meteoglu et al. and Dordevic et al., analyzed histological samples of patients with metastatic RCC and found that the increase in NF-κB (p50) activity correlated with increased angiogenic and apoptotic markers, such as epidermal growth factor receptor (EGFR), VEGF, bcl-2 and p53 [9,13]. An et al. studied the effect of NF-κB blockade with an IkB super repressor, alone and with a proteasome inhibitor (bortezomib), to induce apoptosis in RCC cells. The authors found that specific inhibition of NF-κB was not sufficient to induce apoptosis. However, blocking NF-κB was necessary to induce apoptosis in RCC cells with bortezomib [14]. The impact of inhibiting NF-κB activation by pyrrolidine dithiocarbamate (PDTC) in RCC was evaluated by Morais et al. [1,15,16]. Both, *in vitro* and *in vivo* studies showed that PDTC played a role in inhibition of NF-κB expression and consequently decreased viability and proliferation in RCC.

Endostatin (ES) was originally isolated from hemangioendothelioma and identified as the carboxy-terminal segment of collagen XVIII [17]. ES has become a focus of medical interest because of its tumor angiogenic activity [18]. In 2004, Abdollahi et al. analyzed gene expression in human endothelial cells treated with ES and found that NF-κB was one of the factors influenced by ES in its inhibition of angiogenesis [19].

In recent years, our group has been working with retroviral gene therapy using ES for the treatment of primary and metastatic RCC in animal models. ES showed antiangiogenic and antitumor activities. Furthermore, it was shown that ES caused exhibits potent immunomodulatory effects [20–26].

In this study, we investigated the regulation of NF-κB activity and metastatic Renca-EGFP after ES treatment.

2. Methods

2.1. Cell lines

NIH/3T3-LendSN-clone 3 was utilized for ES expression, and NIH/3T3-LXSN was used as a control, as described in previous work [23,26]. Both cell lines were maintained in high-glucose (4.5 g/L at 25 mM) DMEM medium (Life Technologies Corporation®, Grand Island, NY, USA) supplemented with 100 U/mL penicillin, 100 μg/mL streptomycin (Gibco®), and 10% fetal bovine serum (FBS). The murine kidney carcinoma cell lines (Renca), were purchased from CLS Cell Lines Service® (Eppelheim, Germany). The cells were transfected with enhanced green protein fluorescent (EGFP) maintained in RPMI 1640 medium (Life Technologies Corporation®, Grand Island, NY, USA) and supplemented with 10% fetal bovine serum, 2 mM L-glutamine, 1 mM sodium pyruvate, 1% minimal Eagle's medium nonessential amino acids, 100 U/mL penicillin and 100 μg/mL streptomycin (Gibco®). All the cell lines were maintained in a humidified chamber at 37 °C and under 5% carbon dioxide.

2.2. Animals

Male Balb/c mice (age 8–10 weeks) were obtained from the Animal Facility of IPEN/CNEN-SP, Sao Paulo, Brazil. In these experiments, 35 mice were used (normal = 5, control group = 15, ES-treated group = 15). All animals were cared for in accordance with the standards of the institute under a protocol approved by the Animal Experimentation Ethics Committee (Number of Process: 87/11).

2.3. Orthotopic RCC tumor model

Mice were anesthetized by an intraperitoneal subcutaneous injection of a mixture of ketamine and xylazine (100 mg/kg and 10 mg/kg, respectively). The left kidney was exposed through a left flank incision and was partially exteriorized. Using a Hamilton syringe with a 27-gauge needle, 2×10^5 Renca-EGFP cells in 10 μL of phosphate buffered saline (PBS) were injected under the renal capsule. Then, the kidney was then allowed to fall back into the abdominal cavity. The body wall and the skin incision were closed separately with absorbable 5-0 vicryl sutures. The left kidney was removed by unilateral nephrectomy 7 days after inoculation with the Renca-EGFP cells. The mice were divided into two experimental groups: the control group and the ES-treated group. Each group received a subcutaneous injection of 3.6×10^6 NIH/3T3-LXSN or NIH/3T3-LendSN-clone 3.

2.4. ELISA analysis

At the end of the experiment, blood samples from the mice were taken into test tubes with heparin. Then, the plasma components were separated and frozen at −20 °C. Samples were thawed at the time of the study, and plasma ES levels and NIH/3T3-LendSN-clone 5 levels were measured using a Mouse Endostatin ELISA Kit (Novateinbio® – Accelerates Research and Development – USA) according to the manufacturer's instructions. The ES concentrations were determined at least in duplicate, and the assay reproducibility was confirmed. ELISA plates were read using the Multiskan EX Microplate Reader (Labsystems, Milford, MA, USA).

2.5. Sorting

At the end of the experiment, the metastatic lung tissues were digested with a solution of RPMI and Collagenase A (Roche, Mannheim, Germany) (3:1) to obtain a cell homogenate, which was then submitted to analysis by flow cytometry (BD FACSAria II). We adjusted the size and fluorescence intensity of the red and blue lasers. The initial parameter settings for cell analysis were defined as the "sorting" strategy using the FITC+ (green) cells. These parameters also provided for a homogeneous size distribution

(blue). These cells represent approximately 8% of the total population (calculated from 10,000 events acquired by the equipment).

2.6. Real-time PCR array

RNA extraction and cDNA synthesis: Renca-EGFP cells that passed through the sorting were stored in RNAlater® (QIAGEN, Valencia, CA, USA) at −80 °C until RNA extraction. RNA extraction was performed using a RNeasy® mini kit (QIAGEN, Valencia, CA, USA) following the manufacturer's protocol. After extraction, the concentration of RNA was calculated using a 2000c NanoDrop® (Thermo Scientific), and ∼2 μg of RNA were used for cDNA synthesis using a RT^2 First Strand Kit® (QIAGEN, Valencia, CA, USA). Quantitative real-time PCR: real-time PCR was performed on an Applied Biosystems StepOne Plus® (Foster City, CA) fast real-time PCR system using a PCR Array PAMM 025c-NF-κB Signaling Pathway RT2 qPCR array (SABiosciences, Frederick, MD) according to the manufacturer's instructions. Data were evaluated with the aid of the software available at http://pcrdata-analysis.sabiosciences.com/pcr/arrayanalysis.php.

2.7. Cytoplasmic and nuclear proteins

Approximately 2×10^6 Renca-EGFP cells were homogenized with lysis buffer (10 mM HEPES, 10 mM KCl, 0.1 mM EDTA, 1 mM DTT, 0.1 mM PMSF) together in 10% NP40, left on ice for 15 minutes and centrifuged at 2700 × g for 1 minute. The supernatant, containing the cytosolic protein, was collected and stored at −20 °C. The "pellet" was resuspended in nuclear extraction buffer (10 mM HEPES, 500 mM KCl, 0.1 mM EDTA, 1 mM DTT, 0.1 mM PMSF) and incubated on ice for 15 minutes with vigorous stirring. The mixture was centrifuged 20,000 × g for 5 minutes, and the supernatant containing nuclear proteins was also stored at −20 °C for after analysis.

The concentration of cytoplasmic and nuclear proteins was determined by spectrophotometric reading using the Nanodrop ND-100 (Thermo Scientific®).

2.8. Electrophoretic mobility shift assay (EMSA) and supershift assay for NF-κB

Five micrograms of nuclear extract proteins as incubated with 20 μL of ligation buffer (10 mM Tris-HCl pH 7.5, 1 mM MgCl2, 50 mM NaCl, 0.5 mM DTT, 0.5 mM EDTA; 4% glycerol, 1 μg poly-dldC) for 20 min at room temperature. For this experiment, ∼40,000 counts/min of the double stranded oligonucleotide containing the consensus sequence for NF-κB (5′-AGTTGAGGG-GACTTTCCCAGGC-3′, Sipnase, Sao Paulo, Brazil) labeled with γ - 32P -ATP was added at room temperature for 30 minutes. The DNA-protein complex was analyzed on 6% polyacrylamide gel for 1.5 h at 150 V in Tris-borate EDTA (TBE) buffer. After drying, the gel was exposed to Kodak XAR -5 - (Rochester, New Supershift assay). The supershift analysis was performed using 2 μg/mL anti-p50 antibody, anti-p52, anti-p65, anti-RelB (Abcam, Cambridge, UK) and anti-c-Rel (Santa Cruz Biotechnology Santa Cruz, CA, USA).

2.9. Lung protein extraction

The metastatic lung tissue (100 mg wet weight) was homogenized in 2 mL of extraction buffer (0.1 M Hydroxymethyl Aminomethane, 0.01 M EDTA, 1% sodium dodecyl sulfate (SDS) and 0.01 M Dithiothreitol (DTT) at pH 8.0). After centrifugation at 2000 × g for 10 minutes, the supernatant was collected and stored at −20 °C for later analysis.

2.10. Western blotting

A Mini-Protean® gel 12% (Bio-Rad Laboratories, San Diego, USA) was used for electrophoresis. The total protein (50 μg) was resuspended in Laemmli® buffer with DTT (Bio-Rad Laboratories, San Diego, USA), and a molecular weight standard marker was used (Plus STD Kaleidoscope®, Bio-Rad Laboratories, San Diego, USA) on each gel. The separation run was carried out at 200 V until the bromophenol dye ran off the gel. After electrophoresis, we performed a wet transfer (20 mV for 2.30 minutes) to PVDF membrane (Hybond-ECL®, Amersham Bioscience Pittsburgh®, USA) previously activated with methanol. After transfer, the membranes were washed and incubated for 1 hour in blocking solution containing 5% Bovine Albumin Fraction V powder® (BSA) (Sigma-Aldrich, St. Louis, USA) diluted in TBS. The membranes were incubated with the anti-p50 (Abcam, Cambridge, UK) and anti-Bcl-3 (Santa Cruz Biotechnology Santa Cruz, CA, USA) primary antibodies diluted 1:500 in 5% BSA and 1% goat serum under gentle agitation at 4 °C for 16 hours. For the endogenous control we used anti-β-actin (Abcam, Cambridge, UK). Then, the membranes were incubated with anti-immunoglobulin secondary antibody (IgG) mouse (H + L) conjugated to HRP (Abcam, Cambridge, UK) diluted 1:5000 in 1% BSA under gentle stirring for 1 hour at room temperature. To visualize the protein, we used the SuperSignal® kit (Thermo Scientific, USA), and photo documentation was performed using a Uvitec instrument (Cambridge – Alliance 4.7).

2.11. Histological and immunohistochemistry analyses

The metastatic lung tissue was excised, fixed in methacarn (60% methanol, 30% chloroform and 10% glacial acetic acid) for 3 h and routinely processed for paraffin embedding. Histological analysis was performed in 5 μm sections stained with hematoxylin and eosin (n = 10 animals per group, 10 sections per lung). The samples were analyzed under a light microscopy, and the number of metastatic foci was counted. The quantification was performed at a 400× magnification using the Leica DM1000 (Leica Microsystems, Wetzlar, Germany).

For immunohistochemistry analysis, tissue sections were cut and hydrated. The sections were subjected to antigen retrieval with citrate buffer 10 mM, pH 6.0, in a pressure cooker for 1 min at 125 °C and 25 psi. The slides were blocked with hydrogen peroxide (30 V) and methanol for 30 min. The preparations were blocked for 30 min in a solution containing 5% milk in PBS. Next, the slides were incubated with monoclonal anti-p50 (Abcam, Cambridge, UK) and anti-Bcl-3, (Santa Cruz Biotechnology, Santa Cruz, CA, USA) diluted 1:100 overnight in a humidified chamber at 4 °C. After several PBS washes, the slides were incubated with the reagents supplied by the manufacturers of Novolink Polymer® Detection Systems (Leica Microsystems, Bannockburn, IL), and then we used the diaminobenzine visualization system. The slides were counter-stained with hematoxylin, dehydrated in ethanol, cleared in xylene and mounted using Erv-rmount (EasyPath®, Erviegas, Sao Paulo, SP, Brazil). The images were obtained using a microscope (Leica DM1000), a digital compact camera (Leica DFC420C) and an image processor (Leica Application Suite v3.3.0).

2.12. Immunoprecipitation

Samples with 75 μg of lysate extract nuclear cells were resuspended in PBS to a final volume of 200 μL and were incubated overnight at 4 °C with 2 μg of an anti-p50 (Abcam, Cambridge, UK) and anti-Bcl-3 (Santa Cruz Biotechnology Santa Cruz, CA, USA) antibodies. The anti-mouse IgG (Abcam, Cambridge, UK) antibody was used as a negative control. After 16 hours, the immunoprecipitate was added to protein G-agarose and incubated

with gentle agitation for 4 hours at 4 °C. Then, the immune complexes were centrifuged and were resuspended with 75 μL of buffer ready Laemmli® without DTT (Bio-Rad Laboratories, San Diego, USA), and the sample was heated for 5 minutes at 95 °C in a dry bath. After, the complex was centrifuged at 14,000 × g for 10 minutes at 4 °C and the supernatant was collected.

Western blotting was carried out as previously described. In samples precipitated with anti-p50, western blotting was performed with anti-Bcl-3 and anti-p50. In samples precipitated with anti-Bcl-3, the western blotting was performed with anti-p50 and anti-Bcl-3 as well. Both had two controls samples, two treated with ES, a negative control and a positive control, where the nuclear sample was resuspended in Laemmli buffer ready with DDT.

2.13. Statistical analysis

The results are presented as the mean ± SE. Single comparisons of the mean values were performed by Student's *t*-test. Multiple comparisons were performed using one-way analysis of variance followed by Bonferroni's test using GraphPad Prism, version 4.0 (GraphPad Software San Diego, CA). $P < 0.05$ was considered statistically significant.

3. Results

3.1. ELISA analysis

BALB/c mice were orthotopically injected with murine Renca cells. At the end of the experiment, ES plasma levels in the normal group and experimental groups were measured. The normal group had ES levels of 130.06 ± 13.6 μg/mL, the control group 224.6 ± 35.8 μg/mL and the ES group 317.7 μg/mL ± 36.1. The presence of tumor cells led to an Increase in endogenous ES levels in the control group, and an increase of 1.72-fold compared to the normal group was observed (normal vs. control $P < 0.001$). The ES group had an increase of 2.44-fold compared to the normal group (normal vs. ES $P < 0.001$) and 1.41-fold compared to the control group (control vs. ES $P < 0.001$) (Fig. 1). Circulating ES levels corroborated our previous data [21–26].

3.2. Analysis of gene expression of the signaling pathway of NF-κB

The purity of Renca-EGFP sorted cells, which were used in the first part of this work, was verified by fluorescence microscopy (Fig. 2). Then, NF-κB pathway gene expression profiles were compared between the control and ES-treated group. qRT-PCR showed that only three of 84 genes related to NF-κB-mediated signal transduction were significantly changed after treatment compared to the controls. ES treatment significantly decreased the expression of Bcl-3 (3.56-fold), NF-κB1 (1.95-fold) and c-Rel (3.13-fold) genes compared to the control ($P < 0.001$ and c-Rel $P < 0.004$, respectively).

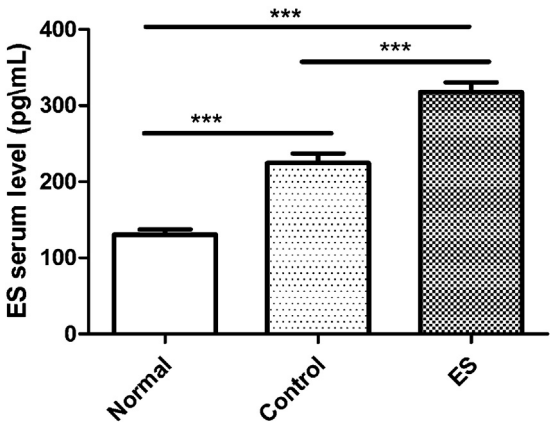

Fig. 1. ES plasma levels were measured in the normal, control and ES groups. The presence of metastases led to a significant increase in the plasma ES levels (normal vs. control group; $^{**}P < 0.001$). However, the ES-treated group showed even higher ES plasma levels [normal vs. ES group, $^{***}P < 0.001$; control group vs. ES group, $^{***}P < 0.001$; analysis of variance (ANOVA) test].

3.3. Identification of NF-κB DNA–binding in the nuclear extracts of Renca-EGFP cells obtained from experimental groups

NF-κB DNA–binding activity was detected in the control and treated group samples. However, in tumor cells in the ES-treated group, we observed a reduction in NF-κB binding activity (Fig. 3A channels 5 and 7). The specificity of NF-κkB DNA–binding complexes was assessed in the presence of excess unlabeled NF-kB oligonucleotides. Complete displacement of the NF-κB DNA–binding complex was observed after the addition of 10 μg of cold NF-κB DNA (Fig. 3A channel 1). Furthermore, the supershift analysis using antibodies against the NF-κB subunits (p50, p52, p65, RelB, and C-Rel) demonstrated that the band correspond to the p50 NF-κB subunit (Fig. 3B, channel 3).

3.4. Effect of ES therapy on the expression of the p50 and Bcl-3 subunits in metastatic lung tissues

Expression of NF-κB1 (p105 and p50) and Bcl-3 in the protein extracts of normal and metastatic lung tissues was verified by western blotting. In the normal lung tissue, expression of p105 and p50 was almost non-detectable. However, in metastatic lung tissue (control and ES-treated groups) expression of p105 and p50 was higher compared to the normal group ($P < 0.001$). Furthermore, treatment with ES resulted in a significant reduction only in the expression of p50 ($P < 0.01$) (Fig. 4A and B) The decrease in p50

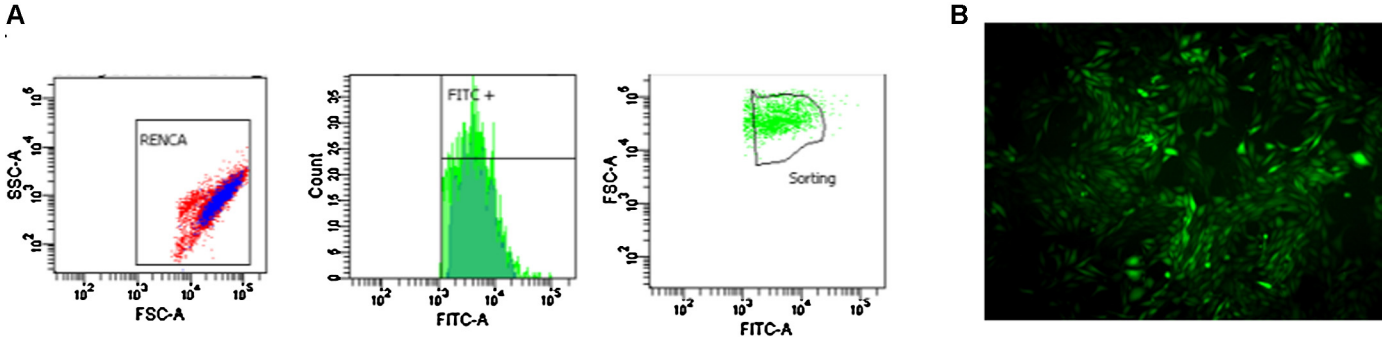

Fig. 2. A. Analysis of Renca-enhanced green protein fluorescent (EGFP) cells after sorting. B. Representative figure of Renca-EGFP cells by fluorescence microscopy.

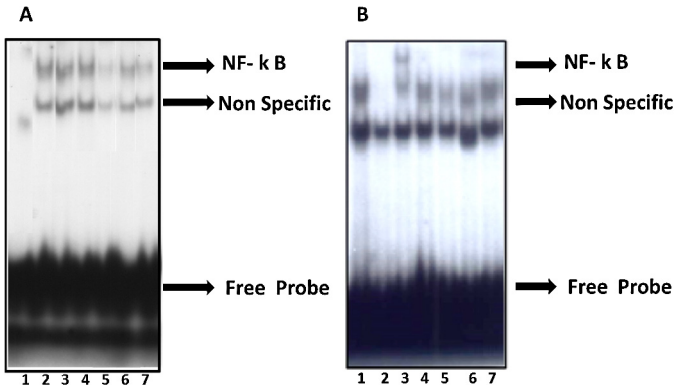

Fig. 3. A. Electrophoretic mobility shift assay (EMSA) analysis of six representative samples of nuclear proteins from tumor cells of control animals and animals treated with ES. Channel 1: assay competition with unlabeled probe; channels 2, 3 and 4: protein samples of tumor cells from the control group; channels 5, 6 and 7: tumor cell protein samples from animals of the group treated with ES. B. Gel shift channel 1: pure nuclear extract, channel 2: competition assay with unlabeled probe; channel 3: nuclear extract incubated with anti-p50; channel 4: nuclear extract incubated with anti-p52; channel 5: nuclear extract incubated with anti-p65; channel 6: nuclear extract incubated with anti-RelB; channel 7: nuclear extract incubated with anti-c-Rel.

from its precursor p105 was established from p50/p105 ratios obtained by scanning densitometric analysis of bands from immunoblots. The ratio given by the average control group was 1.47 ± 0.06, while the treated group was 1.20 ± 0.09 ($P < 0.05$).

The presence of lung metastasis caused an increase in the expression of Bcl-3 (normal vs. control $P < 0.01$). However, treatment with ES did not cause a significant change in the levels of Bcl-3 (Fig. 4A and B).

Expression of p50 and Bcl-3 were further verified by immunohistochemistry. In normal lungs, discrete marking of p50 and Bcl-3 was observed (Fig. 4C, normal group). In the control group, the p50 staining was observed in cytoplasmic and nuclear compartments. In the tumor nodules of the ES-treated group, only the p50 subunit showed reduced intensity of staining in the cytoplasm and nucleus (Fig. 4C, control and ES group). The expression of Bcl-3 was quite evident and unchanged in the nucleus and cytoplasm of metastatic cells compared to the control group and the ES group (Fig. 4C).

3.5. Immunoprecipitation of the p50/Bcl-3 complex

To confirm the physical interaction between p50 and Bcl-3, an immunoprecipitation assay was performed with anti-p50 and anti-Bcl-3, followed by the assessment of the presence of both proteins in the immunoprecipitate. The results presented on Fig. 5 confirm the presence of the p50/Bcl-3 complex in nuclear extracts from Renca-EGFP cells from metastatic lung tissues (Fig. 5). This finding corroborates the results obtained in the supershift gel assay, where we found only one clear shift of the band in the DNA-NF-κB in samples incubated with the p50 antibody (Fig. 3B, channel 3). Additionally, we observed a slight decrease in the signal intensity of p50 and Bcl-3 in the ES group crossed westerns (Fig. 5).

4. Discussion

Changes in the tumor microenvironment following antiangiogenic therapy have yet to be clarified. Hypoxia and nutrient starvation in addition to interactions between stromal and tumor cells modulate the response to antiangiogenic therapy [27]. In this study, we evaluated the modulation of NF-κB in Renca-EGFP cells after gene therapy with ES.

The control group showed plasma levels of ES 1.72 times higher than the normal group. An elevation in the circulating levels of ES also occurs in patients in advanced stages of RCC and can be explained by the action of MMPs and proteases present in the tumor microenvironment. Our data are corroborated by the study of Feldman et al. in 2002, where it was demonstrated that the plasma levels of ES in patients with RCC in stage IV were elevated compared to levels of ES in healthy volunteers [28]. Treatment

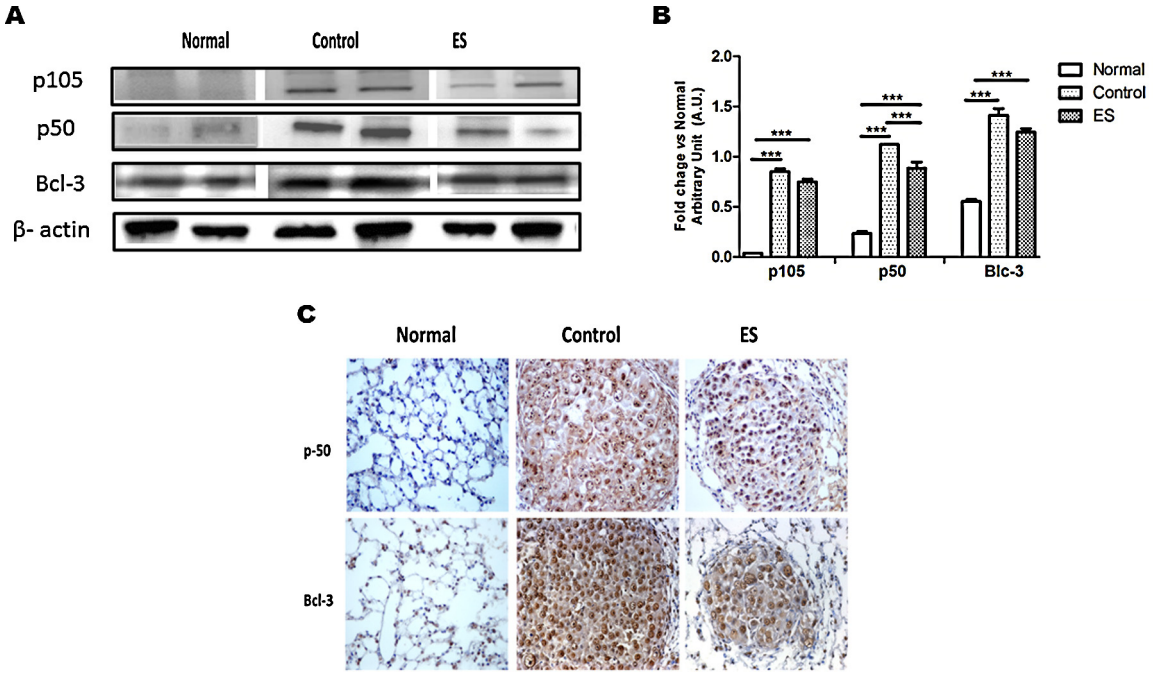

Fig. 4. A. Representative immunohistochemical staining for the p50 and Bcl-3 subunits in metastatic nodules in the lungs of the normal, control and ES animals. B. Western blot of p105 subunits, p50 and Bcl-3 normalized to β-actin. Graph showed that treatment with ES resulted in a significant reduction in the expression of p50 (ES vs. control $^{***}P < 0.01$).

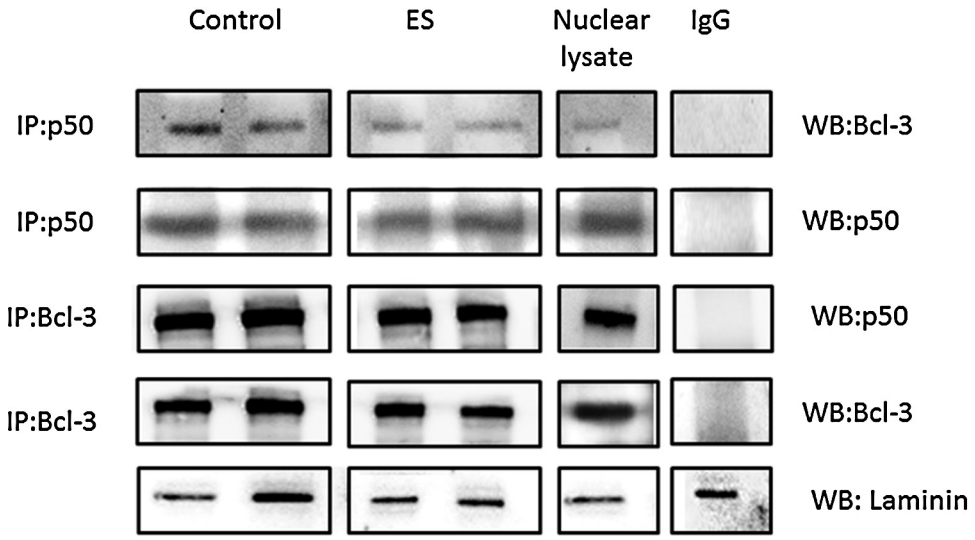

Fig. 5. Immunoprecipitation (IP) of p50 and Bcl-3 nuclear extracts from metastatic lungs. The right panel describes the antibodies used for immunoprecipitation and the left panel describes the antibodies used for the development of western blotting. The total nuclear protein extract was used as a positive control, and as a negative control, we used nuclear extract immunoprecipitated with anti-mouse immunoglobulin secondary antibody (IgG). In the ES group, we observed a slight decrease in signal intensity of p50 and Bcl-3 in western blots.

with gene therapy caused a significant increase in circulating levels of ES, which led to changes in the tumor microenvironment, such as decreases in the number of intranodular vessels and increases in inflammatory infiltrates [21–25]. In turn, these changes lead to changes in the pattern of gene expression in both stromal and tumor cells.

NF-κB represents a central transcription factor in the stress response, proliferation and cell death [29]. Treatment with ES led to decreased expression of genes in the Rel family, such as c-Rel, NF-κB1 and Bcl-3. Moreover, we demonstrated that ES interfered with NF-κB activity in Renca-EGFP cells. Furthermore, our super-shift assay data point to p50 as a major NF-κB regulator that is translocated to the nucleus in Renca-EGFP cells.

The protein profile presented in the lungs of normal mice showed low expression levels of p105, p50 and Bcl-3. However, the presence of tumor cells in the control group promoted a significant increase in all of these proteins. Aberrant activation of NF-κB has been demonstrated in different tumor types including RCC [1,10,29–31]. The p105 and p50 subunits had increased expression in the lungs of control group. However, p50 was the only protein to have decreased protein levels after ES treatment, causing a decrease in the p50/p105 ratio. These findings did not corroborate the results found in RT-PCR, but indicate that treatment with ES affected the proteolytic processing of p105, which resulted in decreased levels of p50. Homeostasis of p105 and p50 appears to be physiologically relevant because transgenic mice expressing p50, but not p105, exhibit severe inflammation. On the other hand, "knock out" NF-κB1 mice do not have significant inflammatory changes. These data indicate that p105 plays an important role in the functional regulation of p50. It is known that the p50/p105 ratio is regulated by post-translational modifications [29].

Immunohistochemical analysis revealed that p50 is present in metastatic nodules in the control group and the group treated with ES. The p50 subunit in the treated group showed less intense cytoplasmic and nuclear staining. These data reinforces the important role of p50 in our model tumor.

Given that Bcl-3 is a co-activator of p50 dimers, we performed an immunoprecipitation assay. Our results confirmed the presence of the p50/Bcl-3 complex in nuclear extracts of the tumor cells of metastatic lungs. The results obtained to date suggest that p50 together with Bcl-3 play a regulatory role in gene transcription in RCC.

Acknowledgements

This study was supported by FAPESP (process number: 2010/18969-0) and CAPES/PNPD (process number: 72-71859).

References

[1] Morais C, Gobe G, Johson DW, Healy H. The emerging role of nuclear factor-kappa B in renal cell carcinoma. Int J Biochem Cell Biol 2011;43:1537–49.
[2] Skolarikos A, Alivizatos G, Lagunab P, Rosett J. A review on follow-up strategies for renal cell carcinoma after nephrectomy. Eur Urol 2007;51:1490–501.
[3] Rini B, Atkins M, Atkins M. Resistance to targeted therapy in renal cell carcinoma. Lancet Oncol 2009;10:992–1000.
[4] Cowey CL, Hutson TE. Molecularly targeted agents for renal cell carcinoma: the next generation. Clin Adv Hematol Oncol 2010;8:357–60.
[5] Huang G, Chen L. Recombinant human endostatin improves antitumor efficacy of paclitaxel by normalizing tumor vasculature in Lewis lung carcinoma. J Cancer Res Clin Oncol 2010;136:1201–11.
[6] Dolcet X, Llobet D, Pallares J, Matias-Guiu X. NF-κB in development and progression of human cancer. Virchows Archiv 2005;446:475–82.
[7] Karin M. NF-κB as a critical link between inflammation and cancer. Cold Spring Harb Perspect Biol 2009;11:5.
[8] Gilmore TD. Introduction to NF-κB: players, pathways, perspectives. Oncogene 2006;25:6680–4.
[9] Meteoglu L, Erdogdu IH, Meydan N, Erkus M, Barutuca S. NF-kappa B expression correlates with apoptosis and angiogenesis in clear cell renal cell carcinoma tissues. J Exp Clin Cancer Res 2008;27:53.
[10] Thornburg NJ, Pathmanathan R, Raab-Traub N. Activation of nuclear factor-kappa B p50 homodimer/Bcl-3 complexes in nasopharyngeal carcinoma. Cancer Res 2003;63:8293–301.
[11] Oya M, Ohtsubo M, Takayanagi A, Tachibana M, Shimizu N, Murai M. Constitutive activation of nuclear factor-κB prevents TRAIL-induced apoptosis in renal cancer cells. Oncogene 2001;20:3888–96.
[12] Oya M, Takayanagi A, Mizuno R, Ohtsubo M, Marumo K, Shimizu N, et al. Increased nuclear factor-kappa B activation is related to the tumor development of renal cell carcinoma. Carcinogenesis 2003;24:377–84.
[13] Dordevic G, Matusan-Ilijas K, Sinozci E, Damante G, et al. Relationship between vascular endothelial growth factor and nuclear factor-κB in renal cell tumors. Croat Med J 2008;49:608–17.
[14] An J, Sun Y, Fisher M, et al. Maximal apoptosis of renal cell carcinoma by the proteasome inhibitor bortezomib is nuclear factor-kB dependent. Mol Cancer Ther 2004;3:727–36.
[15] Morais C, Healy H, Johson DW, Gobe G. Inhibition of nuclear factor-kappa B attenuates tumour progression in an animal model of renal cell carcinoma. Nephrol Dial Transplant 2010;25:1462–74.

[16] Morais C, Gobe G, Johson DW, Healy H. Inhibition of nuclear factor-kappa B transcription activity drives a synergistic effect of pyrrolidine dithiocarbamate and cisplatin for treatment of renal cell carcinoma. Apoptosis 2010;15:412–25.
[17] Oh SP, Warman ML, Seldin MF, Cheng SD, Knoll JHM, Timmons S, et al. Cloning of cDNA and genomic DNA encoding human type XVIII collagen and localization of the α1(XVIII) collagen gene to mouse chromosome 10 and human chromosome 21. Genomics 1994;19:494–9.
[18] Lin Y, Zhang S, Rehn M, Itaranta P, Tuukkanen J, Heljasvaara R, et al. Induced repatterning of type XVIII collagen expression in ureter bud from kidney to lung type: association with sonic hedgehog and ectopic surfactant protein. C. Development 2001;128:1573–85.
[19] Abdollahi A, Hahnfeldt P, Maercker C, Grone HJ, Debus J, Ansorge W, et al. Endostatin's antiangiogenic signalling network. Mol Cell 2004;13:649.
[20] Coutinho EL, Andrade LNS, Chammas R, Morganti L, Schor N, Bellini MH. Antitumor effect of endostatin mediated by retroviral gene transfer in mice bearing renal cell carcinoma. FASEB J 2007;21:3153.
[21] Rocha FG, Chaves KC, Chammas R, Peron JP, Rizzo LV, Schor N, et al. Endostatin gene therapy enhances the efficacy of IL-2 in suppressing metastatic renal cell carcinoma in mice. Cancer Immunol Immunother 2010;59:1357–65.
[22] Rocha FG, Chaves KC, Gomes CZ, Barrichelo CC, Courrol LC, Schor N, et al. Erythrocyte protoporphyrin fluorescence as a biomarker for monitoring antiangiogenic cancer therapy. J Fluoresc 2010;20:1225–31.
[23] Chaves KCB, Foguer K, Peron JPS, Pesquero JB, Schor N, Turaça LT, et al. Endostatin gene therapy stimulates upregulation of ICAM-1 and VCAM-1 in a metastatic renal cell carcinoma model. Cancer Gene Ther 2012;8:558–65.
[24] Chaves KCB, Dagli MLZ, Mennecier G, Pesquero JB, Schor N, Turaça LT, et al. Fibronectin expression is decreased in metastatic renal cell carcinoma following endostatin gene therapy. Biomed Pharmacother 2012;66:464–8.
[25] Braga MS, Chammas R, Chaves KC, Schor N, Bellini MH. Endostatin neoadjuvant gene therapy extends survival in an orthotopic metastatic mouse model of renal cell carcinoma. Biomed Pharmacother 2012;66:237–41.
[26] Braga MS, Chammas R, Chaves KC, Foguer K, Pesquero JB, Schor N, et al. Vascular endothelial growth factor as a biomarker for endostatin gene therapy. Biomed Pharmacother 2013;67:511–5.
[27] Murakami M, Zhao S, Zhao Y, Chowdhury NF, You W, et al. Evaluation of changes in the tumor microenvironment after sorafenib therapy by sequential histology and 18F-fluoromisonidazole hypoxia imaging in renal cell carcinoma. Int J Oncol 2012;41:1593–600.
[28] Feldman AL, et al. Prospective analysis of circulating endostatin levels in patients with renal cell carcinoma. Am Cancer Soc 2002;95:1637–43.
[29] Demarchi F. Glycogen synthase kinase-3 beta regulates NF-kappa B1/p105 stability. J Biol Chem 2003;10:39583–90.
[30] O'Neil BH, Buzkova P, Farrah H, Kashatus D, Sanoff H, Goldberg RM, et al. Expression of nuclear factor-kappa B family proteins in hepatocellular carcinomas. Oncology 2007;72:97–104.
[31] Sourbier C, et al. Targeting the nuclear factor-kappa B rescue pathway has promising future in human renal cell carcinoma therapy. Cancer Res 2007;67:11668–76.